

EFFECTS OF CLAMPING ON THE LASER FORMING PROCESS

Paper # 102

Andrew J. Birnbaum., Peng Cheng, Y. Lawrence Yao

Columbia University
500 W. 120 st., New York, NY, 10027, United States

Abstract

Although considerable effort has gone into characterizing the laser forming process in terms of process parameters and conditions, there has been little emphasis on the effects of the mechanical and thermal constraints introduced by the clamping method utilized for a desired application. This research suggests means for investigating and predicting the resulting geometry of a specimen due to laser operation in close proximity to an array of imposed thermo-mechanical constraints for single scan applications; specifically, the resulting average bending angle as well as bending angle variations along the laser scanning path. This is accomplished by initially only considering these effects on the thermal field. Conclusions are then drawn about the nature of the mechanical effects. These conclusions are validated through numerical simulation as well as physical experimentation.

1. Introduction

The laser forming process involves the local/concentrated input of energy through the use of a defocused laser, moving at a relative velocity to a thin-sheet work piece of varying geometric complexity. This local energy input results in a non-uniform transient temperature distribution, giving rise to thermally induced stresses, strains and permanent deformations. Through proper control over process parameters such as laser velocity, power, beam spot size, path geometry, and clamping method, final part geometries as well as material characteristics may be controlled to an acceptable degree of accuracy.

Laser forming is classified as a non-traditional manufacturing process, as it does not require any externally applied forces to generate desired forms. This is the main advantage it has over its traditional counterparts, as the hard tooling process has been eliminated from the overall process flow. This also introduces a considerable degree of flexibility, as hard tooling has in effect been replaced by virtual means, in that process parameters, as well as path geometry may

be altered at any time to create totally new forming conditions.

Much effort has been made in characterizing the underlying mechanisms for the process. Vollertsen [1] has identified three main mechanisms which give rise to various types of deformation, while Mucha et. al [2] provided analytical formulations of the mechanical process, and Bao and Yao [3] address final deformation characteristics, specifically edge effects which are highly relevant to this research.

Though much has been determined with respect to the underlying mechanisms for deformation as well as the aggregate effects of varying process parameters, little effort has been put forth in studying the effects of part fixturing. Work holding is seen as a major issue for many traditional manufacturing processes. Fixture design and analysis, as well as its impact on the process it is applied have all received much attention. Methods for increasing the efficiency of overall process flow with respect to effective work holding have also been explored [4]. Work holding "ideologies" like the 3-2-1 locating scheme have even been developed. Fixturing method also has significant effects on post process material characteristics including residual stresses, microstructure, warpage and distortion. For example, Wang and Pelinescu [5], through a contact analysis studied the work-piece-fixture contact force for a general clamp-support-locator configuration, Karafillis and Boyce [6] examined the post process "spring back" effect in sheet metal forming, while Roy and Liao [7] investigated work piece stability issues for a virtual disturbance on a given fixture-work piece configuration.

Although, as mentioned above, laser forming is an extremely flexible process in that no hard tooling is required, a method for maintaining desired part location and orientation is still required. However, the degree to which parts may be constrained is also quite flexible. For example, the V-block configuration used by Edwardson et. al [8] consists simply of a platform which the part lays on, with a V-shape cutout to freely allow bending deformation of thin sheet coupons. Jones [9] employs the use of a cooling bed, which

serves as a platform on which the part rests, but is given total freedom to deform as the platform itself is flexible and free to deform. Further constraint may be necessary though if complex three dimensional scan paths are used. For these cases it may be necessary to provide a method such as edge or corner clamping to provide the necessary part orientation with respect to the laser.

In terms of application, the two practical methods that have emerged require that either the part be fixed while the laser moves relative to it or the reverse situation where the laser is static and the part is translated or rotated by an x-y stage or robotic manipulation through predetermined paths. The research herein examines in depth, the effects of both the method of fixturing utilized as well as the effects of laser operation in close proximity to an applied external constraint, such as an edge-clamp. Lee and Lin [10] has recognized the potential impact of operating close to an applied constraint. Although he does not specifically explore these issues, he does go about choosing an operating distance that he deems sufficiently great from the clamp so as to minimize these potential effects.

As will be seen in the following sections, both the clamping method utilized and the distance to a constraint will affect final deformation characteristics in the form of average bending angle, as well as bending angle distributions along the laser scan path. This study also examines these effects for an array of process parameters, thereby providing a set of practical guidelines for application by enabling these factors to be taken into account when determining laser path geometries and heating conditions.

2. Overview of Approach

This research examines the edge-clamped, and the so-called free case, where there is no externally applied constraint other than the provision of a flat surface for support (Fig. 1). With the assumption that the process is sequentially coupled, i.e. the stress and strain fields are both functions of the transient temperature distribution, while the effect of the stress and strain field on the temperature is negligible, the problem may be decomposed into a purely thermal, and thermo-mechanical analysis. As stated above, effects of the method of clamping are investigated as well as the effects of operating at varying distances from a free or clamped edge. Figure 2 shows a schematic of the model considered where straight line laser paths parallel to the clamped or free edge at perpendicular distances 'a' are examined. It is

assumed that at sufficiently large values of 'a', both the thermal and mechanical fields are unaffected by the presence of the clamped or free edge. However, as the distance of operation is reduced, there will be

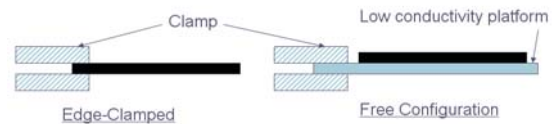


Figure 1: Schematic of clamped and unclamped configurations.

some threshold value of 'a' where the presence of that discontinuity will cause a perturbation in the behaviour of the model. In fact there will be two distinct operational regions, excluding the unperturbed case. One where the mechanical field will be affected while the thermal field remains unaffected, and a second at an even further reduced distance where there will be a coupling of effects due to the mechanical and thermal field both "feeling" the presence of the discontinuity in material.

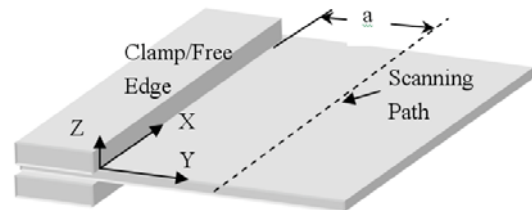


Figure 2: Schematic of clamped specimen specifying coordinate system and operating distance.

This is a central concept in terms of analysis, as this enables the isolation and study of purely mechanically induced behaviours as long as the process is operating at distances greater than the threshold. Results of finite element analyses suggest that the mechanical field will be perturbed well before that of the thermal field. Practically, this seems logical as plastic deformation in the laser forming process occurs on a relatively short time scale. This serves to further decrease the effective thermal threshold distance. This suggests that even at small operational distances where the time history, or cooling phase after the laser has passed will surely be affected, it will have a relatively minor effect on the actual final deformation, at least for single scan applications. However, this time history, or cool down phase effect will have implications for multiple scan applications, where the thermal field from previous scans may need to be taken into account for future ones.

3. Experimental Conditions

Experiments were conducted with a CO₂ laser with a maximum 1500 W power output, with a Gaussian intensity distribution. The laser system remained stationary while a precision XY platform translated the specimens along the desired straight path and velocity. Edge-clamped specimens were clamped at one end cantilevering the specimen (Fig. 1). The clamp material in contact with the specimen is of low thermal conductivity as to inhibit enhanced conduction keeping the thermal field comparable to that of the unclamped case. The unclamped specimens were supported from underneath by a low conductivity wood block (Fig. 1). The Temperature Gradient Mechanism (TGM) is dominant in the present study. This is ensured through the proper choice of heating conditions.

All specimens are square 80 mm edge length, 0.89 mm thickness coupons of low carbon steel AISI 1010. Samples are treated to remove surface inconsistencies and then coated with graphite to enhance laser power absorption. Constraint induced phenomenon are of central interest for the current study, requiring isolation of the distance to the free or clamped edge, and the clamping method as the only variable parameters. All specimens are subjected to an applied power of 800 W at a beam spot diameter of 4mm, at a velocity of 50 mm/s along a straight scanning path. Both the clamped and free specimens were run at distances of 40 mm (center scan), 25 mm and 10 mm from the free or clamped edge. Local deformations including bending angles were determined through the use of a precision coordinate measuring machine (CMM).

4. Numerical Analysis

For this research, both the rigidly constrained (edge-clamped) and free (unclamped) cases were modeled. As this is a coupled thermo-mechanical analysis, both thermal and mechanical constraints are required. It is assumed however, that the coupling is sequential. This enables solving the thermal model independently, and using the solution data (transient temperature distributions) as inputs to the mechanical model.

For the thermal model, both clamp-type models are subjected to the same surface/boundary conditions; convection is specified on all plate surfaces, while a moving circular heat source with a Gaussian power distribution specified by a user defined FORTRAN script, simulates the effect of the laser. The

temperature dependence of thermal conductivity and specific heat is also taken into account. The governing equation is therefore the temperature dependent classical heat equation with convective sources:

$$\rho \cdot C_p(T) \cdot \frac{\partial T}{\partial t} = \nabla(k(T)\nabla T) + \sum h_i(T - T_\infty) \quad (1)$$

The mechanical models take into account both the dynamics of the process and non-linear geometric effects stemming from large deformation theory. The temperature dependence of material properties including Young's Modulus, coefficient of thermal expansion and flow stress are taken into account as well. It is assumed that the total strain and strain rate may be decomposed into elastic, plastic, creep and thermal components of strain and strain rate in an additive manner by: $\dot{\epsilon}_{tot} = \dot{\epsilon}_{el} + \dot{\epsilon}_{pl} + \dot{\epsilon}_{th}$ where the contribution from creep is not considered due to the relatively short time scale over which deformation occurs. Flow stress is also modelled with a dependence on strain and strain rate. Elastic strains are calculated through an isotropic Hooke's Law, whereas the onset of yielding in the simulations is determined by the Von Mises criterion,

$$[(\sigma_1 - \sigma_2)^2 + (\sigma_2 - \sigma_3)^2 + (\sigma_1 - \sigma_3)^2] / 2 = \sigma_y^2 \quad (2)$$

where σ_y is the temperature dependent flow stress determined from a uni-axial tension test. Further, the resultant plastic strain is governed by the flow rule:

$$d\epsilon_{ij} = d\lambda \frac{\partial f}{\partial \sigma_{ij}} \quad (3)$$

where σ is stress, ϵ is strain, $d\lambda$ is the instantaneous proportionality constant and $f = f(\sigma_{ij})$ is the yield function. In this case, the Von Mises criterion is used as the appropriate yield function $f(\sigma_{ij})$. The strain dependence of flow stress is modelled as:

$$\sigma_y = K\epsilon^n \quad (4)$$

where K is the strength coefficient, and n, the strain hardening component. Strain rate dependence of flow stress is given by:

$$\sigma_y = C\dot{\epsilon}^m \quad (5)$$

where C is the strength coefficient, and m is strain rate sensitivity exponent, also a temperature dependent

parameter. Although the strain hardening and rate sensitivity components may be determined, the empirical relationships suggested by Vashchenko et. al [11] and Maekawa et. al [12] have been adopted as they directly incorporate temperature, strain and strain rate dependence:

$$\sigma_y = \sigma_s + (8.2 + 1.3\dot{\varepsilon} \cdot e^{-0.0135\dot{\varepsilon}}) * (0.97e^{0.0007\dot{\varepsilon}}) \cdot (1.14 - 0.0023 \cdot T) \quad (6)$$

for $293 K < T < 573 K$, where σ_s is the static flow stress at 293 K, and

$$\sigma_y = A(T, \dot{\varepsilon}) \left(\frac{\dot{\varepsilon}}{1000} \right)^{0.0195} \dot{\varepsilon}^{0.21} \quad T > 573 K \quad (7)$$

where

$$A(T, \dot{\varepsilon}) = 1394e^{-0.0011T} + 339 * \exp(-0.0000184T - (943 + 23.5 \ln \frac{\dot{\varepsilon}}{1000})^2) \quad (8)$$

Implementation of these material property relationships within the simulation is accomplished through the use of a temperature and strain rate dependent yield stress ratio:

$$R(T, \dot{\varepsilon}) = \frac{\bar{\sigma}}{\sigma_s} \quad (8)$$

where $\bar{\sigma}$ is the strain rate dependent flow stress. The strain and temperature dependence is first taken into account and then multiplied by the appropriate yield stress ratio for the rate dependent effect.

Numerical models contain between 2400 and 4200 20-node quadratic elements; DC3D20 for the thermal case, and C3D20 for the mechanical case in ABAQUS. These higher order elements, although more computationally expensive, prevent shear locking and hour-glass effects associated with their eight node counterparts, and are therefore necessary for this, a bending-dominated deformation process Cheng and Yao[13]. Attention is given to specifying a fine mesh resolution at and near the scanning path, while away from the scanning path there is a fairly coarse mesh density.

The clamped case requires the specification of zero displacement in the Y and Z direction along one full edge, and restriction of X displacements at two nodes to inhibit rigid body motion. The decision to constrain only the Y and Z displacements is due to the

fact that although there is some constraint in the X direction, it is well below that of the Z, whereas the Y restriction serves as a reference about which the entire part may expand or contract. This is supported by Postacioglu et. al [14] who specifically addresses this point. Furthermore, models including a constraint in the X direction were unable to capture several experimentally observed trends.

The unclamped case requires that only rigid body displacement and rotation be constrained as it is attempting to simulate an essentially un-constrained condition. This is accomplished by specifying zero X, Y and Z displacement on two nodes located at the center of the laser scanning path at the mid plane and bottom surface. This constrains X, Y, and Z rigid body displacement, and rotation about the X and Y axes. One further node, located at the end of the scanning path on the bottom plane is constrained to zero displacement in the Y direction to inhibit rotation about the Z axis.

5. Results and Discussion

Simulations were performed at each of three different velocities, for three different powers and three distinct operational distances for both the clamped and unclamped cases. Figures 3a,b, and 4a-d show representative experimental and numerical results at for both the average bending angle magnitude, and bending angle distributions. It is seen that both the experimental magnitudes and trends are captured quite well by the numerical results. Upon this validation of the numerical model, several more sets of simulations were run at two additional velocities and powers.

5.1 Average Bending Angle

The treatment for the analysis of both the numerical and experimental results will be divided into that of average bending angle magnitude, and bending angle distribution along the laser scan path. Beginning with the former, it is seen in Figures 3a,b that for both the clamped and unclamped cases, the average bending angle decreases with decreases in operating distance from the clamped or free edge. The slope of the bending angle function for both cases also exhibits a dramatic change as the distance 'a' is decreased from 25mm to 10mm, as opposed to the functional behaviour between 40mm and 25mm. This therefore represents a transition, with respect to the average bending angle, from the unperturbed situation to one where the presence of the clamped or free edge is

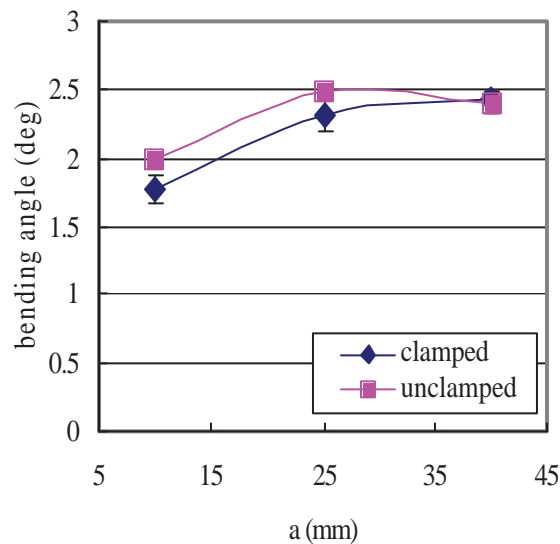


Figure 3a: Experimental, Average Bending Angle as a function of operating distance. ($Q=800\text{W}$, $v=50\text{ mm/s}$)

“felt” in a mechanical sense, though the thermal field remains unaffected. The slight discrepancy between the experimental numerical clamped results is most likely due to the fact that the clamped condition is modelled as a mathematically rigid constraint, while in reality there is some compliance associated with the clamp in both the Y and Z directions.

In examining the mechanical aspects of the process, it is important to distinguish between two types of mechanical constraint. The first is an inherent mechanical constraint due purely to the geometric characteristics of the part. It is well established that plastic strain along the direction perpendicular to the scan path is directly linked to the magnitude of the average bending angle and is caused by the locally heated volume of material being constrained by the relatively cold surrounding material. The extent to which this cold material inhibits local thermal expansion is the level of inherent constraint being applied to the heat affected zone. A larger level of inherent constraint will result in enhanced plastic strain in the Y direction and therefore an increase in local, and average bending angle. The second is an applied external constraint provided, for example, by the presence of an edge clamp. It will be seen that for operation within the presented processing window, inherent constraint plays the dominant role in governing the final average bending angle magnitude, while the external constraint, effectively, plays almost none at all. The decrease in average bending angle as the operating distance reduces is due to a decrease in the inherent constraint (in the Y direction) as a free or clamped edge is approached.

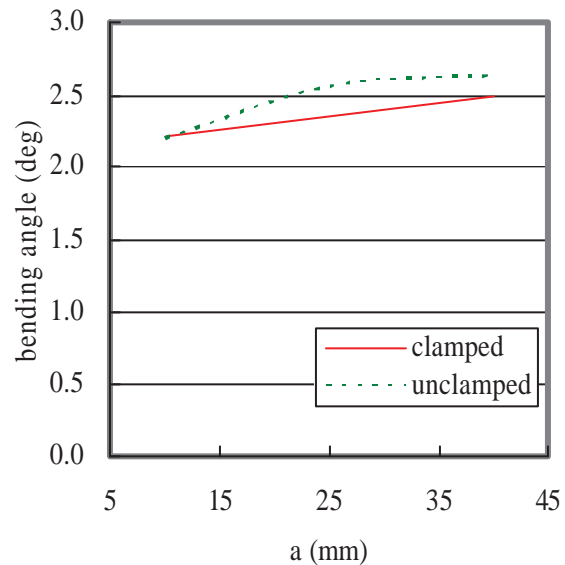


Figure 3b: Numerical, Average Bending Angle as a function of operating distance. ($Q=800\text{W}$, $v=50\text{ mm/s}$)

The reason for this reduction in constraint stems from the fact that the edge being approached is traction free. Therefore, instead of a large volume of material providing a relatively rigid surrounding, the material adjacent to the traction free surface now is able to expand much more freely. This in turn results in less plastic strain and therefore a lower bending angle. The metric chosen to express this reduction in constraint is the instantaneous spatial integral of the elastic normal stress distribution in the Y direction (σ_{yy}). This integration is performed along a path perpendicular to the scanning direction at a typical interior section at the instant the laser passes this location. Further, only the compressive components of stress are taken as a measure of inherent constraint, as this is de facto what is providing the resistance to thermal expansion at that particular instant. Figure 5 shows a typical plot of σ_{yy} or constraint as a function of Y for three different operating distances. It is obvious from the plot that the total component of compressive (integral of the negative portions of the curve) normal stress decreases as operational distance decreases. It is seen from Figure 6 that within the process window of parameters simulated, the elastic constraint for the unclamped case decreases monotonically with: decreases in operating distance, decreases in power and increases in velocity. The clamped case has the same qualitative functional dependence on elastic constraint. Figures 7a,b show average bending angle decreasing monotonically in the same manner as that of the elastic

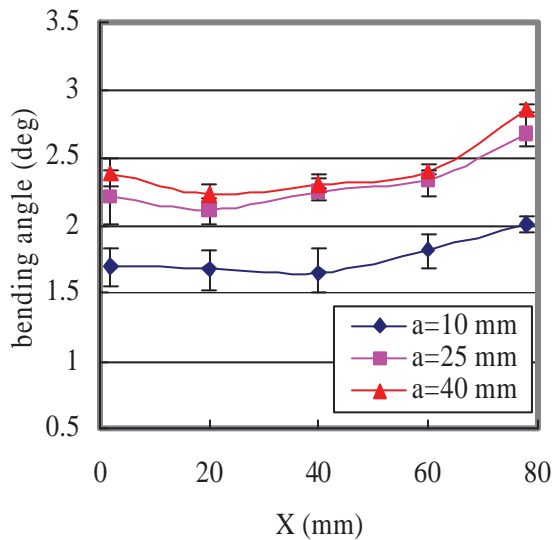


Figure 4a: Clamped, Experimental Bending Angle Distribution. (Q=800 W, v=50 mm/s)

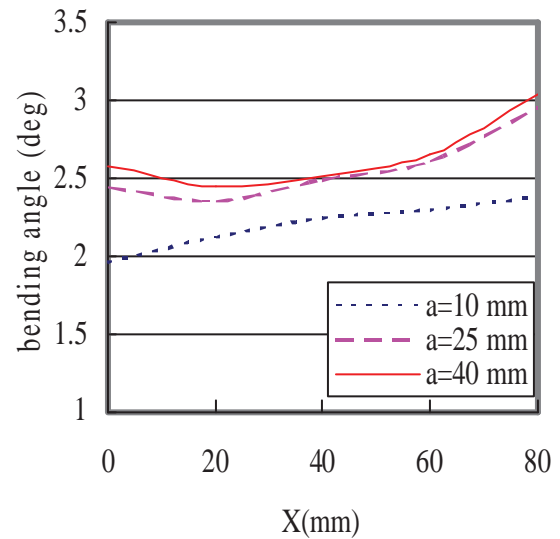


Figure 4b: Clamped, Numerical Bending Angle Distribution. (Q=800 W, v=50 mm/s)

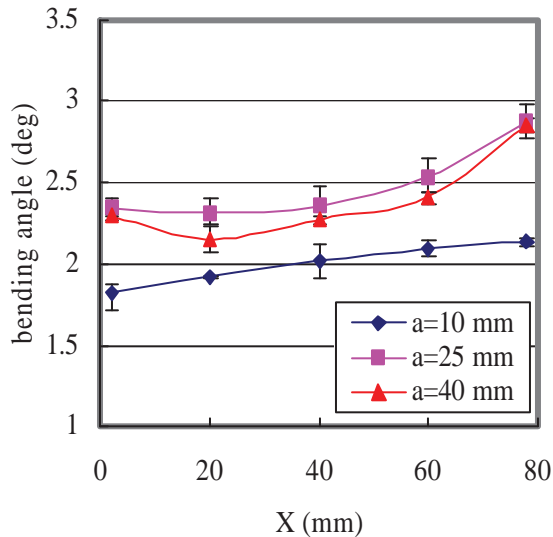


Figure 4c: Unclamped, Experimental Bending Angle Distribution. (Q=800 W, v=50 mm/s)

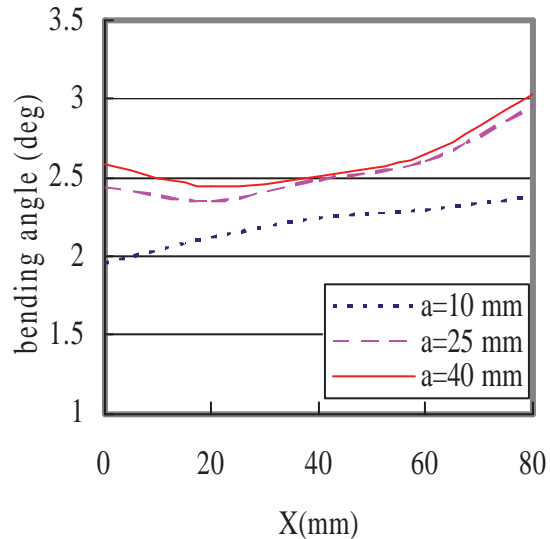


Figure 4d: Unclamped, Numerical Bending Angle Distribution. (Q=800 W, v=50 mm/s)

constraint with respect to changes operating distance, power and velocity. This suggests that changes in inherent constraint with respect to changes in process parameters is a valid explanation for the observed behaviour in average bending angle magnitude for both the clamped and unclamped cases. A comparison between the clamped and unclamped cases may also be made. Figure 8 shows a typical plot of σ_{yy} vs. Y for the clamped and unclamped cases operating at the same powers, velocities and distances from the edge. It is seen that the stress distributions remain consistent until the clamped edge is approached.

This deviation is a Poisson induced stress stemming from the presence of the clamp, which acts to inhibit displacement in the Z direction. This would suggest that the presence of this external constraint would act to increase the total level of constraint, thus causing an increase in bending angle. However, it is seen that although the clamped specimens have much higher constraint values, the average bending angles for the unclamped configuration are greater in many cases. Although there is an increase in externally applied constraint, the presence of the clamp also

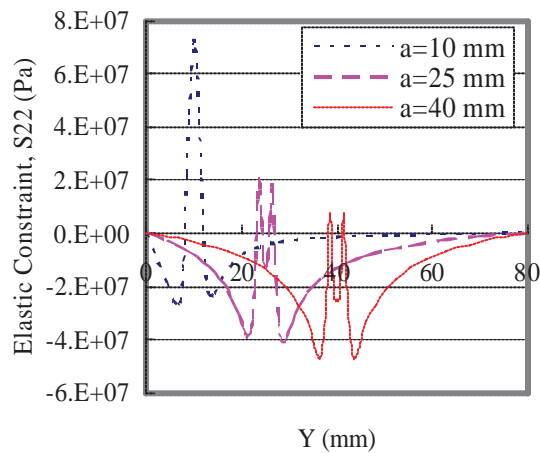


Figure 5: Comparison of elastic constraint for three operating distances. (Unclamped, $Q=960$ W, $v=70$ mm/s)

introduces a competing effect by increasing the effective bending rigidity about the X axis. This is seen by examining the instantaneous σ_{yy} distribution at the bottom surface of the specimen as the laser passes this location. Figure 9 shows a dramatic increase in elastic constraint for the clamped case relative to the unclamped as the operating distance is decreased. However, Figure 9 also shows a corresponding increase in instantaneous σ_{yy} across the part in the bottom surface of the clamped specimen. These competing effects introduced by the presence of the clamp provide an explanation for the above mentioned discrepancy between the clamped and unclamped cases in average bending angle magnitudes.

5.2 Bending Angle Distribution

Bending angle distribution refers to the variation in local bending angle along the laser scan path. The bending angle is calculated from relative Z displacements along paths at fixed Y distances from, and parallel to, the laser scan path (Fig. 10). The locations of these paths relative to the scan path are chosen to lie outside of the heat affected zone so as to avoid any local distortions, and are the same for both the clamped and unclamped cases for each distinct operating distance. The total local bending angle is calculated from the addition of the two angles generated on either side of the scanning path. The volume of material adjacent to the clamp, or for unclamped cases, the smaller section, will be termed the minor region, and the other, the major. The metric chosen to quantify the variation in bending angle is the curvature of the bending angle vs. X function. Curvature is approximated by fitting a second order

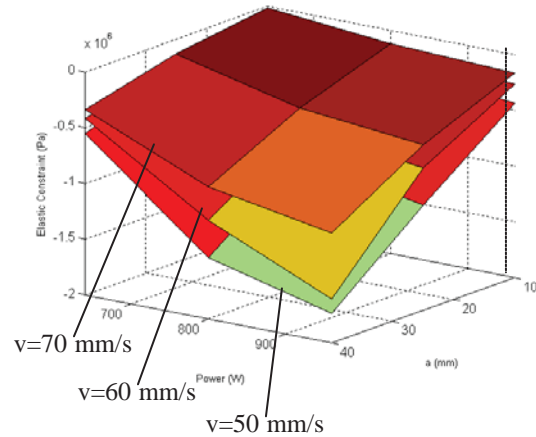


Figure 6: Unclamped, Elastic Constraint as a function of power and operating distance for

polynomial through the desired function. It is important to note that the variation in bending angle is not equivalent to the variation in displacement along the part.

The bending angle curvature results from the *relative* curvatures in Z displacement along sampling paths. Therefore, an increase in relative curvature of the displacements along sampling paths results in an increase in bending angle curvature magnitude, and thus greater variation in local bending angle along the scan path. The sign of curvature refers only to the curvature direction, with a concave down instance being arbitrarily chosen as negative. This also implies that a negative bending angle curvature will have a larger relative displacement within the part relative to the edges, whereas a positive curvature implies a larger relative difference at the part edges.

In order to isolate the effects of changes in operating distance, the unclamped case will first be examined to exclude the effects of any external constraint. Figure 11 is a typical plot of bending angle curvature as a function of operating distance. It is seen that for both the clamped and unclamped cases, curvature strictly increases with increases in operating distance for both the clamped and unclamped cases.

The slope of the curvature function for both cases also exhibits a dramatic change as the distance 'a' is decreased from 25mm to 10mm, as opposed to the functional behaviour between 40mm and 25mm. The variation in Z displacement as a function of X is due to bending about the Y axis induced by elastic and plastic strains in the X direction, as well as

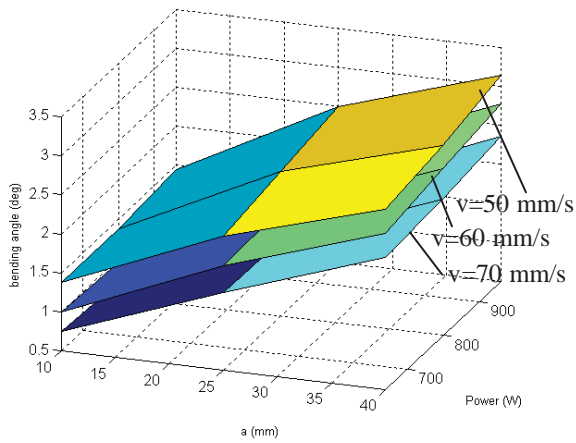


Figure 7a: Clamped, Numerical, average bending angle as a function of operating distance and power for three velocities.

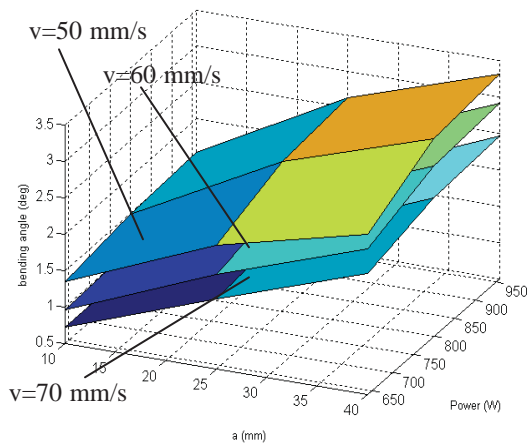


Figure 7b: Unclamped, Numerical, average bending angle as a function of operating distance and power for three velocities.

non-uniform plastic strain in the Y direction along the scanning path. Upon consulting the numerical results, it is seen that the former has a minimal effect on the final Z displacement, as the total X strain

($d\epsilon_{el} + d\epsilon_{pl}$), remains relatively constant through the thickness of the part, and thus contributes mostly to a uniform shrinkage in the X direction. The latter is therefore the major contributor to variations in Z displacement along sampling paths. The change in plastic strain in the Y direction as a function of X (Fig. 12) along the scan path is again due to changes in inherent constraint. However, as opposed to the average bending angle study, the distribution is affected by changes in constraint due to the presence

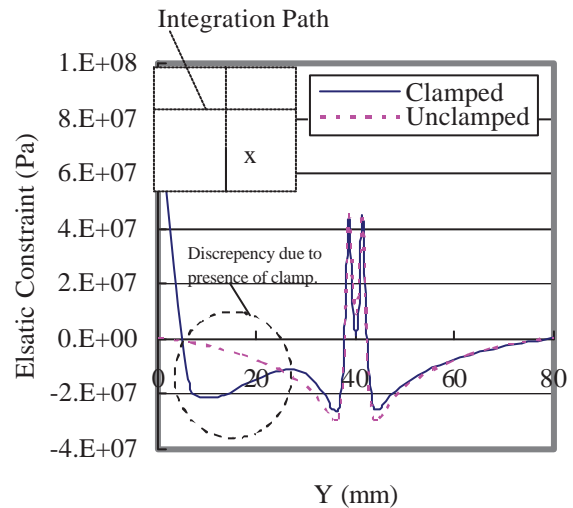


Figure 8: Comparison of clamped and unclamped σ_{yy} (constraint) distribution. (Q=800 W, v=60 mm/s, a=40 mm)

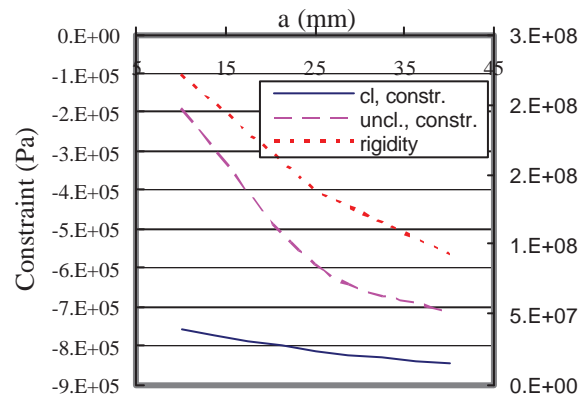


Figure 9: Typical comparison of total elastic constraint in the top surface between clamped and unclamped configurations. (Q=800 W, v=60 mm/s). Also shown is the instantaneous stress at the bottom layer of the part, showing a dramatic increase in effective bending rigidity as operating distance decreases. (right scale)

of the edges *perpendicular* to the scanning path. Upon entering or exiting (X=0, and X=W respectively) the part, the volume of material heated by the laser experiences much less constraint due to a reduced volume of surrounding “cold” material. These edge effects will give rise to variations in Z displacement along all paths parallel to the scanning path. The functional dependence of displacement curvature on operating distance is also explained by changes in inherent constraint, as according to numerical results,

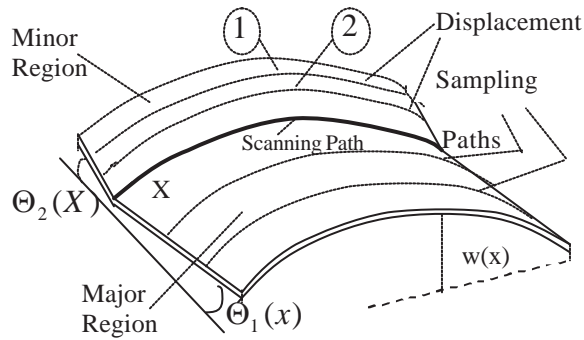


Figure 10: Portrayal of major and minor regions, sampling path locations, major and minor bending angles and local Z displacement, $w(x)$.

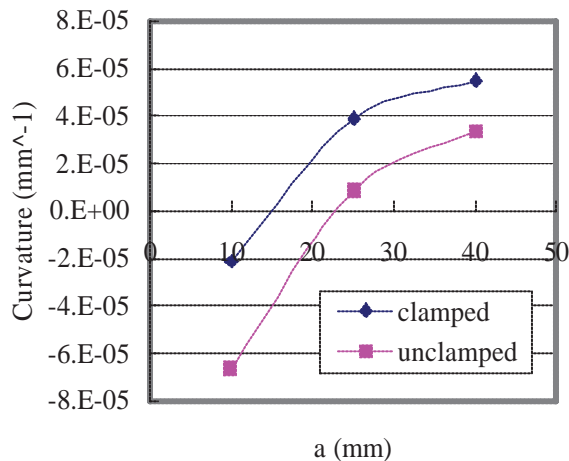


Figure 11: Representative curvature comparison between clamped and unclamped configurations. ($Q=640$ W, $v=60$ mm/s)

plastic and elastic strain in the X direction along the scanning path are not functions of operating distance, and remain constant.

As explained in the previous section on average bending angle, a decrease in operating distance results in a decrease in constraint due to the presence of a free edge parallel to the scanning path, and therefore a reduction in plastic strain in the Y direction. In this case, the reduction in constraint due to the presence of a free edge parallel to the scanning path *relative* to the reduction in constraint due to the edges perpendicular to the scanning path is the source of the functional dependence. For example, the $a=10$ mm, and $a=40$ mm case have effectively the same reduction in constraint due to the edges perpendicular to the scanning path. However, the $a=10$ mm case is

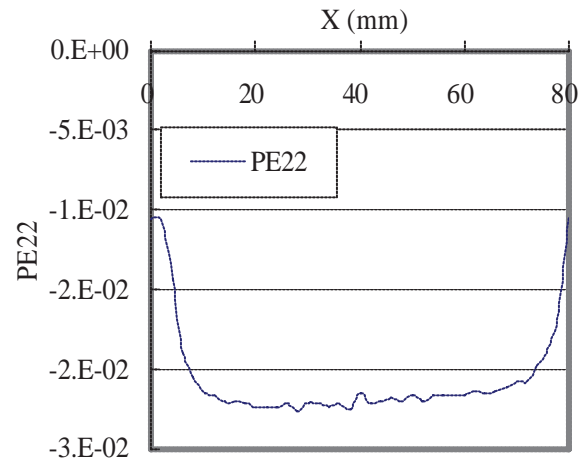


Figure 12: Plastic strain in the Y direction as a function of X. Note the decrease in magnitude at both edges.

associated with a much reduced quasi-steady level of inherent constraint due to the proximity of the free edge parallel to the scan path. This reduction in relative difference in inherent constraint results in a smaller variation in Z displacement along paths parallel to the scanning path and therefore reduces the bending angle curvature.

The clamped case may be explained through the same line of reasoning as that of the unclamped. Again, plastic and elastic strains in the X direction are constant through the part thickness, are not functions of operating distance and are equal to those of the unclamped cases. This is due to the fact that the clamp mainly serves to inhibit Z displacement. Figure 11 also serves as a typical plot, and shows that bending angle curvature in the clamped case is greater than its unclamped counterpart for all operating distances. This may again be explained by differences in relative displacement curvatures. Figure 13 shows a typical plot of Z displacements along sampling paths in the minor section for the $a=40$ case. It is seen that the presence of the clamp greatly inhibits not only displacement magnitude but *variation* in displacement as well; particularly for the sampling path closer to the clamp. Although the displacements have been greatly reduced, the difference in displacement curvature has increased substantially, thus causing a higher bending angle curvature than that of the unclamped case. Numerical results also indicate that bending angle curvature for both the clamped and unclamped cases.

6. Conclusion

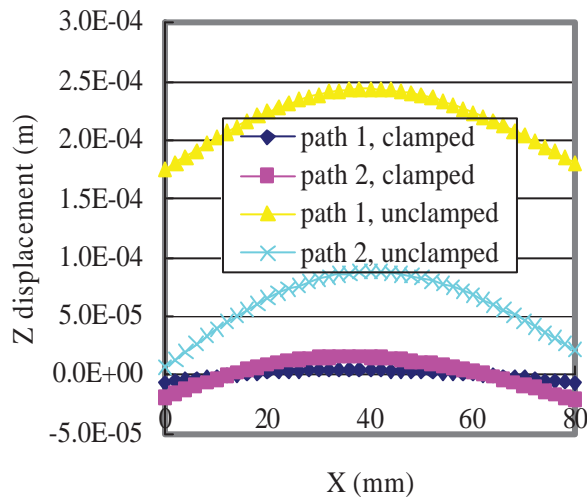


Figure 13: (Numerical Results) Comparison of relative displacement curvatures in minor region. (a=40 mm, Q=640 W, v=60 mm/s)

In terms of the average bending angle, the presence of the clamp results in minimal deviation from that of the free case. This is due to the competing effects of increases in constraint, but increases bending rigidity as well. However, the effect of operating in close proximity to a clamped or free edge will have dramatic effects on final deformation and should be taken into account in application. Similarly, for bending angle distribution, the operating distance will have a considerable effect on the final variation in bending angle along the scanning path. The presence of the clamp will also serve to change the bending angle distribution by increasing the relative displacement curvatures and thereby causing larger variations compared to the unclamped configuration.

Acknowledgements

The authors acknowledge the support of NIST under grant number ATP-00005269.

References

- [1]Vollertsen, F. (1994) Mechanisms and Models for Laser Forming, Laser Assisted Net Shape Engineering, Proceedings of the lane '94, Vol. 1, pp.345-360.
- [2]Mucha, Z., Hoffman, J., Kalita, W. and Mucha, S. (1997) Laser Forming of Thick Free Plates, Laser Assisted Net Shape Engineering, Proceeding of the Lane'97, pp.383-392.
- [3]Bao, J., and Yao, Y.L. (2001) Analysis and Prediction of Edge Effects in Laser Bending, J. Manufacturing Science and Engineering, ASME, Vol. 123, pp.53-61.
- [4]Hoffman, E.G. (1996) Setup Reduction Through Effective Work Holding, Industrial Press Inc. New York, NY.

- [5]Wang, Y.W. and Pelinescu, D.M.(2002) Prediction of Workpiece-Fixture Contact Forces Using the Rigid Body Model, Publication Source Unknown.
- [6]Karafilis, A.P. and Boyce, M.C. (1992) Tooling Design in Sheet Metal Forming Using Springback Calculations, Intl. J. Mech. Science, Vol. 34, No. 2, pp.113-131.
- [7]Roy, U. and Liao, J. (2002) Fixturing Analysis for Stability Consideration in an Automated Fixture Design System, ASME, J. Manufacturing Science and Engineering, Vol. 124, pp.98-104.
- [8]Edwardson, S.P., Watkins, K.G., Abed, E. Bartkowiak, K. and Dearden, G. (2005) Geometrical Influences on the Bend Angle Rate per Pass During Multi-Pass 2D Laser Forming, *Proc. IWOTE'05*, Intl. Workshop on Thermal Forming, pp. 29-46
- [9]Jones, J.E., (2005) Internal Communications, NATEchnology.
- [10]Lee, K. and Lin, J. (2002) Transient Deformation of Thin Metal Sheets During Pulsed Laser Forming, *Optics & Laser Technology*, 34, pp.639-648.
- [11]Vashchenko, A.P., Suntsov, G.N., Belalova, G.V. and Medvedev, A.A. (1991) Mechanical Properties of Low Carbon Steel Over a Wide Range of Temperature and Strain Rates Applied to Processes of Thin Sheet Rolling, *Strength Mat.*, 22, pp.1205-1214.
- [12]Maekwa, K Shirakashi, T. and Usui, E. Flow Stress of Low Carbon Steel at High Temperature and Strain Rate (part 2)-Flow Stress Under Variable Temperature and Variable Strain Rate, *Bull. Jpn. Soc. Precis. Eng.*, 17, pp.167-172.
- [13]Cheng, J. and Yao, Y.L. (2001) Cooling Effects in Multiscan Laser Forming, *J. Man. Proc. SME*, Vol. 3, No.1, pp.60-72.
- [14] Postacioglu, N., Kapadia, P., and Dowden, J.M. (1997) Thermal Stresses Generated by a Moving Elliptical Weldpool in the Welding of Thin Metal Sheets, *J. Phys., D: Appl.Phys.*, pp. 2304-2312.

Meet the Authors

Andrew J. Birnbaum is a Ph.D candidate in the Department of Mechanical Engineering at Columbia University. He received a BS in 2002 and a MS in 2004 in Mechanical Engineering from Carnegie Mellon University.

Peng Cheng is a Ph.D candidate in the Department of Mechanical Engineering at Columbia University. He received a BS in 1997 and a MS in 2000 in Mechanical Engineering from Tsinghua University, China.

Y. Lawrence Yao is a Professor in the Department of Mechanical Engineering at Columbia University. He received his Ph.D. from the University of Wisconsin-Madison in 1988. He serves on the Board of Directors of LIA.